SPACE TELESCOPE SCIENCE INSTITUTE
Operated for NASA by AURA

Instrument Science Report WFPC2 00-03

Update on Charge Trapping and CTE Residual Images in WFPC2

S. Baggett, J. Biretta, and J.C. Hsu
September 18, 2000

ABSTRACT

We provide an update on the status of charge trapping in the WFPC2 CCDs, as measured from the strength of residual images in dark calibration frames taken after external science images. The new images support the original finding that the amount of charge trapped appears correlated with the maximum intensity clocked through the pixel during readout (Biretta & Mutchler, 1998). The charge in the residual image is found to be given roughly by ln(residual)~0.36ln(Imax), where Imax is the geometric mean of the maximum pixels in each residual image column. Furthermore, the amount of charge seen in the residual images appears to have been stable over the six years. This stability is in marked contrast to the evolving CTI (charge transfer inefficiency) found via photometry of external stellar images (e.g., Whitmore et al., 1999) and analysis of cosmic ray tails in dark frames (Riess et al., 1999). Finally, there is evidence that these residuals can be relatively long-lived: some residuals appear in darks started more than 20 minutes after the external image was read out.

Introduction

CTI (charge transfer inefficiency) results in targets losing charge as they are clocked out. The effect is most pronounced for objects near the top (Y~800) of the chip: the more rows the target must be clocked through, the more charge is lost. The problem has been attributed to impurities in the silicon which trap the charge, preventing it from being read out immediately (Holtzman et al., 1995). During the first on-orbit calibrations early in

WFPC2's mission, the Investigation Definition Team (Holtzman et al., 1995) discovered the presence of CTI in the CCDs and at that time, with an operating temperature of -76^{o} C, the CTI was measured at ~10-15%. Lowering the operating temperature reduces the CTI, so the camera temperatures were set as low as possible, -88^{o} C, which reduced the CTE (charge transfer efficiency) losses to ~3-4% in the worst case (top of the chip, in 1994). After the acquisition of several more years of calibration data, the CTI was found to be increasing over time (Whitmore & Heyer, 1997). Stellar aperture photometry of Omega Cen showed that the CTE loss for faint stars (20-50DN in a 2 pixel radius aperture, filter F814W, a-to-d gain 15) at the top of the chip had gone from 3+/-3% in 1994 to 22+/-3% in 1997, while the CTE loss over time had remained stable for brighter stars (≥ 200 DN). A later study (Whitmore et al., 1999) confirmed that the CTE losses continue to increase for faint stars: up to 40% in February 1999 though again, the CTE loss for bright targets appears stable. The effect appears to be correctable, using the X- and Y-positions of the targets, the count levels in the background, the brightness of the stars, the date of the observation, and the formulae given in Whitmore et al., 1999.

Charge in the WFPC2 overscan has also been used as a means of measuring CTE in the serial register or X-direction (Mutchler, et al., 1998). An excess in the overscan above the nominal bias level was detected, implying a decay time scale (half-life for charge release) of about 10 microseconds. And, the excess has increased since the installation of WFPC2 though the level of excess doesn't appear to correlate with the image intensity. In this case, the effect was attributed to possible charge trapping in the serial register though other possible causes (e.g., amplifier hysteresis or CTE due to CCD electronics) could not be ruled out.

More recently, cosmic ray trails in dark frames have been found to be a useful tracer of the time dependent X- and Y-CTE (Riess et al., 1999). As for the stellar photometry, the counts in the cosmic ray trails (CRTs) depend strongly on their chip location as well as on the background, source counts, and observation date. The CRT analysis confirmed the suspicion that some of the charge lost via CTI is re-released on relatively short time scales (tens of milliseconds, equivalent to a few pixels distance) though not all of the charge lost is recovered in these short tails.

In addition, hot pixels have been used to measure CTI effects (Biretta et al., 2000). From a high SNR image of an average hot pixel (700 hot pixels from a dozen WFPC2 dark calibration frames), three distinct components of CTE were identified: fast-decay tails (decay scale ~1 pixel) due to both parallel and serial transfers, and a very long extended tail (~30 pixels), not seen before, from parallel transfers. Due to their long decay length, the extended tails are highly effective in displacing signal from typical photometry apertures; they appear to account for much of the photometric CTE loss in WFPC2 stellar images. Measurements of the parallel transfer tails as a function of hot pixel intensity shows that the quantity of trapped charge is roughly 1.2 I**0.37, where I is the pixel intensity (in DN), which reproduces the stellar photometry CTE losses to within a few percent.

Investigations into a CTE component with a long dissipation time scale (minutes) have also been completed (Biretta & Mutchler, 1997). That study took advantage of the occasional residual images detected in darks after external images (Biretta et al., 1995). The data indicated that the amount of trapped charge in a pixel was correlated with the maximum intensity clocked out in the external image, with a dissipation timeliest for the trapped charge of about 16 minutes.

In this study, we expand upon the original residual image analysis and search for any hint of evolution over time as has been seen in other CTE components, by using the additional data taken since the last study. We also refine the measurement method for the residuals in the dark calibration frames. In addition, we search for hints of a residual bulk image component.

Data

The HST data archive was mined for all images of solar system targets (“moving targets”) which were followed by dark frames begun no more than 8 minutes after the external image readout. As with the original study (Biretta & Mutchler, 1998), we began by searching for planetary images because they typically have high exposure levels which generate residuals that extend over many pixels. However, since the number of images was still relatively small, particularly at the later epochs, we also searched for other non-proprietary extended targets (such as planetary nebulae) that were closely followed by darks.

The images collected are summarized in Table 1. Listed for each external image is the image rootname, exposure start time, exposure time, target name, a-to-d gain, CCD containing the target image, and number of saturated pixels in that camera. Also listed is the dark frame following the external image, time delay between external image readout and start of dark exposure, median of the residual (in DN), and geometric mean of the maximum intensity in the external image (in units of gain 7 DN). Shaded rows mark observations that were ultimately not included in the final analysis due, e.g., to excessive number of saturated pixels where the maximum intensity can no longer be reliably determined.

Appendix A contains mosaics of some of the external and dark images listed in Table 1. Typically, the darks show a residual image at the location of the target in the external image, and also extending down the CCD in the readout direction. The intensity level (Imax) in the external images was computed by first finding the maximum pixel value in each column, then taking the geometric mean of these maxima in different columns containing the target. The range of residual columns used was defined by the FWHM of the maximum pixel intensity profile.

The darks, at either 1800 sec or 1000 sec, are normally much longer than the external images and suffer from a considerable number of cosmic ray hits. To reduce the resulting noise in the darks and facilitate measurement of the residual above the surrounding dark level, the dark frames were median filtered. The filter was a sliding window of 5x5 pixels,

moved across the image, with the center pixel in the window assigned the median value of the pixels in the window. The residual charge level above the dark current background level was then measured from an average of the residual charge rows in the median-filtered images. The dark background level was measured in the areas outside of the residual area, though avoiding the droop areas at the CCD edges; error bars on the background level were approximated as the spread in measurements taken from several different regions. The uncertainty in the background level was typically the dominant term in the residual image intensity uncertainty.

Table 1: Inventory of extended target images followed closely by dark frames[a].

External Images							Dark Frames			
rootname	**exposure start time**	**exptime (sec)**	**target**	**gn**	**CCD**	**sat. pixels**	**rootname of dark[b]**	**delay (min)**	**median of residual**	**ln(Imax)**
u2d3010ct	49468.0849	10.00	Ida	7	1	0	u28u1i01t	5	0.03	5.27
u2g00902t0	49530.0731	800.00	CometSL	7	1	7	u28u2o01t	5	0.01	5.17
u2g00602t	49547.6412	800.00	CometSL	7	3	1947	u2en5609t	5	0.56	8.11
u2g00602t	49547.6412	800.00	CometSL	7	3	1947	u2en5609t	5	0.27	7.92
u2g00602t0	49547.6412	800.00	CometSL	7	1	3	u2en5609t	5	0.01	4.75
u2g00604t	49547.7044	1000.00	CometSL	7	3	2399	u2en560at	5	0.48	8.29
u2h50205t	49587.9731	6.00	Mars	7	1	576	u2fd2a01t	5	0.38	8.03
u2fi2k0bt	49588.9391	0.11	Jupiter	15	3	0	u28u3t01t	5	0.32	8.46
~~u2fi2l0dt~~	~~49589.0057~~	~~60.00~~	~~Jupiter~~	~~7~~	~~3~~	~~0~~	~~u28u3u01t~~	~~5~~	~~0.27~~	~~7.35~~
u2n20303t	49785.7391	700.00	Jupiter	7	1	2	u28u7r01t	5	0.14	5.40
u2h50b05t	49815.8203	4.00	Mars	7	1	150	u2en100at	5	0.25	7.79
u2p60407t	49894.5953	40.00	Europa	15	1	221	u2fd8e01t	5	0.59	8.58
~~u2qe0107t~~	~~49901.4335~~	~~500.00~~	~~Uranus~~	~~7~~	~~1~~	~~17~~	~~u28ua501t~~	~~4~~	~~0.19~~	~~5.90~~
u2tf0104t	49938.7835	260.00	Sat(moon)	7	4	37	u2ry0m01t	5	0.54	7.92
u2tf0108t	49938.8467	400.00	Sat(moon)	7	4	7	u2ry0n01t	5	0.19	6.54
u2sa5204t	49957.0641	2.00	IC4593	15	1	1	u2ry1401t	5	0.20	8.07
~~u2wv0309t~~	~~49986.5544~~	~~16.00~~	~~Jupiter~~	~~7~~	~~1~~	~~8~~	~~u2ry1u01t~~	~~5~~	~~0.92~~	~~7.36~~
u2wc0202t0	50021.7439	1500.00	Saturn	7	3	11	u2ry2n01t	5	0.20	5.45
u2sa6202t	50048.3683	100.00	A34	15	1	2	u2ry3a01t	5	0.49	8.44
u315010st	50065.8627	400.00	CometSL	0	--	0	u2ol0i0bt	0	0.00	0.00
~~u32z0507t~~	~~50196.2537~~	~~400.00~~	~~Jupiter~~	~~7~~	~~3~~	~~3~~	~~u2ry6s01t~~	~~5~~	~~0.54~~	~~4.32~~

Table 1: Inventory of extended target images followed closely by dark frames[a].

External Images							Dark Frames			
rootname	**exposure start time**	**exptime (sec)**	**target**	**gn**	**CCD**	**sat. pixels**	**rootname of dark[b]**	**delay (min)**	**median of residual**	**ln(Imax)**
u38m020dt	50209.8564	23.00	Vesta	15	1	0	u2ry7501t	5	0.57	8.53
u38m020qt	50209.9203	23.00	Vesta	15	1	0	u2ry7601t	5	0.64	8.68
u3b10203t0	50258.1759	800.00	Jupiter	7	3	17	u2ry8301t	5	0.15	5.36
u3fw0504t	50329.4224	160.00	Jupiter	7	3	0	u2ry4x01t	5	0.20	6.80
u3du030at	50349.1856	7.00	CometHB	7	1	2	u2ry6901t	5	0.07	6.00
u35t2908t	50349.3773	400.00	PK321+02D1	7	1	7	u2ry6801t	4	0.12	6.27
~~u3ap0310t~~	~~50377.4731~~	~~6.00~~	~~Jupiter~~	~~15~~	~~1~~	~~108~~	~~u2ry1k01t~~	~~5~~	~~0.99~~	~~8.32~~
u3in0205t	50384.2537	30.00	Titan	7	2	0	u2ry8801t	7	0.10	6.32
u3ev4702t	50395.3787	260.00	LMC-SMP42	7	1	8	u2ry8o01t	5	0.02	4.69
u450010cm	50682.0349	1000.00	KBobj.	7	1	4	u43i3a01m[b]	6	0.16	5.24
u450010em	50682.1029	1000.00	KBobj.	7	3	13	u43i3b01m[b]	5	0.19	6.29
u4500302m	50682.1696	1000.00	KBobj.	7	3	7	u43i3c01m[b]	5	0.05	7.84
u450040dr	50683.0432	1100.00	KBobj.	7	3	21	u43i3d01r[b]	5	0.20	7.99
u450040er	50683.0946	1000.00	KBobj.	7	3	21	u43i3e01r[b]	5	0.00	7.39
u3jj5a0er0	50701.9932	1200.00	Saturn	7	3	8	u43i4y01r[b]	5	0.10	5.70
u3jj5a0hr	50702.0731	100.00	Saturn	7	1	13541	u43i4z01r[b]	5	0.38	8.39
u4980204r	50714.0571	2.60	Mars	7	1	0	u43i5z01r[b]	6	0.16	7.69
u43h0408r	50737.0772	400.00	Uranus	7	1	2	u43i7v01r[b]	5	0.17	6.13
u4020406r	50781.0168	40.00	PKS1004+13	7	2	2	u43ibj01r[b]	5	0.36	7.04
u4020306r	50850.1120	40.00	PKS0736+01	7	2	2	u43ihb01r[b]	5	0.20	6.86
u4wd130or	51010.9953	8.00	Jupiter	15	1	0	u476c101r[b]	8	0.20	8.85
u4wd130or	51010.9953	8.00	Jupiter	15	3	186	u476c101r[b]	8	0.22	8.64
u54u010gr	51116.9897	500.00	PK112-001	7	2	12	u4772701r[b]	7	0.01	5.29
u35t1408r	51223.0842	200.00	PK285-02D1	7	1	21	u477b301r	4	0.07	6.84
u58r010fr	51240.0321	0.70	Mars	7	1	0	u477cg01r[b]	5	0.29	7.46
u58r020fn	51240.0995	0.70	Mars	7	1	0	u477ci01r[b]	5	0.36	7.43
u58o040cr	51296.0522	2.00	Mars	7	1	2	u477h501r[b]	6	0.20	7.66

Table 1: Inventory of extended target images followed closely by dark frames[a].

External Images							Dark Frames			
rootname	**exposure start time**	**exptime (sec)**	**target**	**gn**	**CCD**	**sat. pixels**	**rootname of dark[b]**	**delay (min)**	**median of residual**	**ln(Imax)**
u5hh5006r	51372.0196	400.00	PK060-07D2	7	1	19	u5iv0u01r	5	0.30	6.17
u5hh5306r	51413.0661	400.00	PK130-11D1	7	1	17	u5iv1p01r	5	0.09	5.00
u5hh1306r	51413.6509	300.00	PK352-07D1	7	1	16	u5iv1s01r	5	0.24	7.10
u3aw0601m	51413.8578	0.40	Europa	15	1	0	u5iv1u01r	5	0.48	8.12
u5hh0106r	51414.0731	400.00	PK165-06D1	7	1	16	u5ix2g01r[b]	5	0.07	6.46
u5gq1109r	51415.0904	0.40	Saturn	7	1	0	u5ix2k01r[b]	5	0.38	7.63
u5gqa106r	51415.1397	40.00	Saturn	7	1	16	u5ix2l01r[b]	7	0.39	7.40
u3awb801r	51423.1460	0.50	Io	15	1	0	u5ix3801m[b]	5	0.21	8.29
u5hh5806r	51445.1113	230.00	PK300-02D1	7	1	23	u5ix5201r[b]	5	0.22	4.93
u5hh5506r	51447.1224	400.00	PK235-01D1	7	1	19	u5ix5701r[b]	5	0.03	5.82
u5hh1906r	51448.0585	400.00	PK226-03D1	7	1	20	u5iv2j01r	5	0.03	4.14
~~u5hp020br~~	~~51465.1752~~	~~60.00~~	~~Jupiter~~	~~7~~	~~3~~	~~14~~	~~u5ix6r01r~~[b]	~~5~~	~~0.32~~	~~7.63~~
u5hh2306r	51600.0960	400	PK024-+031D1	7	1	0	u61f4901m	5	0.03	4.93

a. Shaded and crossed out rows mark observations that were not included in the final fits. Shaded rows contain observations with excessive numbers of saturated pixels in the regions of interest. Crossed out entries are images that may have been adversely affected by residuals from an external image preceding the external image/dark pair.

b. Darks flagged with ‘b’ were 1000 sec instead of the usual 1800 sec.

Results

As in the original study, we find that the residual image intensity is correlated with the maximum intensity clocked through the pixel. Figure 1, left plot, presents the maximum intensity profile (maximum intensity in each column) for an external image overplotted with the average profile (average target intensity in each column). On the right is the average of the residual charge rows in the corresponding (median-filtered) dark. The residual profile traces the maximum intensity level, including the asymmetry, quite well; in contrast, the shape of the average intensity profile is not obviously reflected in the residual. Appendix B provides the maximum intensity profile plots for all external images and plots of all average residual charge rows in the associated (median-filtered) darks, in the order presented in Table 1.

Figure 1: Left: the maximum intensity in external image (solid line) and average intensity distribution over the target only (dashed line). Right: the average of the residual charge rows in the following (median-filtered) dark.

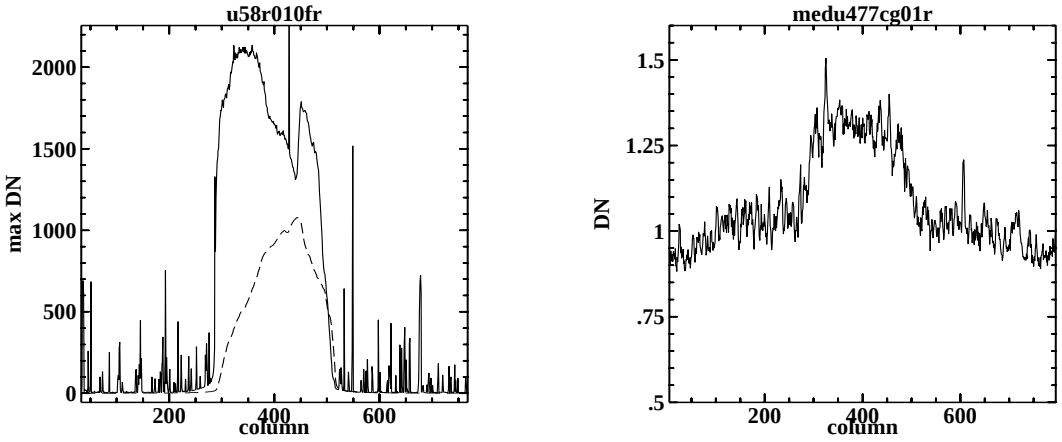

Upon examination of all the external image profile plots and their accompanying dark residual patterns, it became clear that some of the profile plots did not match the residual pattern in the dark very well. In those cases, we generated the Imax profile of the image that preceded the external / dark image pair and found that often, the residual pattern appeared to match the earlier profile better than it matched the profile from the image immediately preceding the dark. The plots to the left in Figure 2 illustrate a time-sequence of three images: an image of Jupiter in F218W (u32z0506t, read out 20 minutes before the dark was taken), followed by an image of Jupiter in F160BW+F130LP (u32z0507t, read out 5 minutes before the dark was taken), followed by an 1800 sec dark (u2rv6s01t). As seen in the figure, even though the time delay between the first external and the dark was much longer than the time between the second external and the dark, the residual in the dark matches the first external profile (u32z0506t). The set of images to the right in Figure 2 illustrate a similar effect: the dark appears to contain a residual from the preceding

image (u3awb801r, an image of Io read out 5 minutes before the dark began) as well as a residual from the image taken even earlier (u3awa801r, an image of Ganymede, read out 19 minutes before the dark began). Since Io and Ganymede fell on mostly different columns in the chip, the residuals in the dark don't overlap much and appear as two separate peaks in the residual. Images that may have been adversely affected by residuals from an external image preceding the external / dark pair were excluded from the fit and have been crossed out with a line in Table 1.

Figure 2: The maximum intensity in the two external images (top and middle plots) preceding the average of the residual charge rows in the associated median-filtered dark (bottom plot). Left plots are for the Jupiter case, right plots are for the Io/Ganymede case, as discussed in the text.

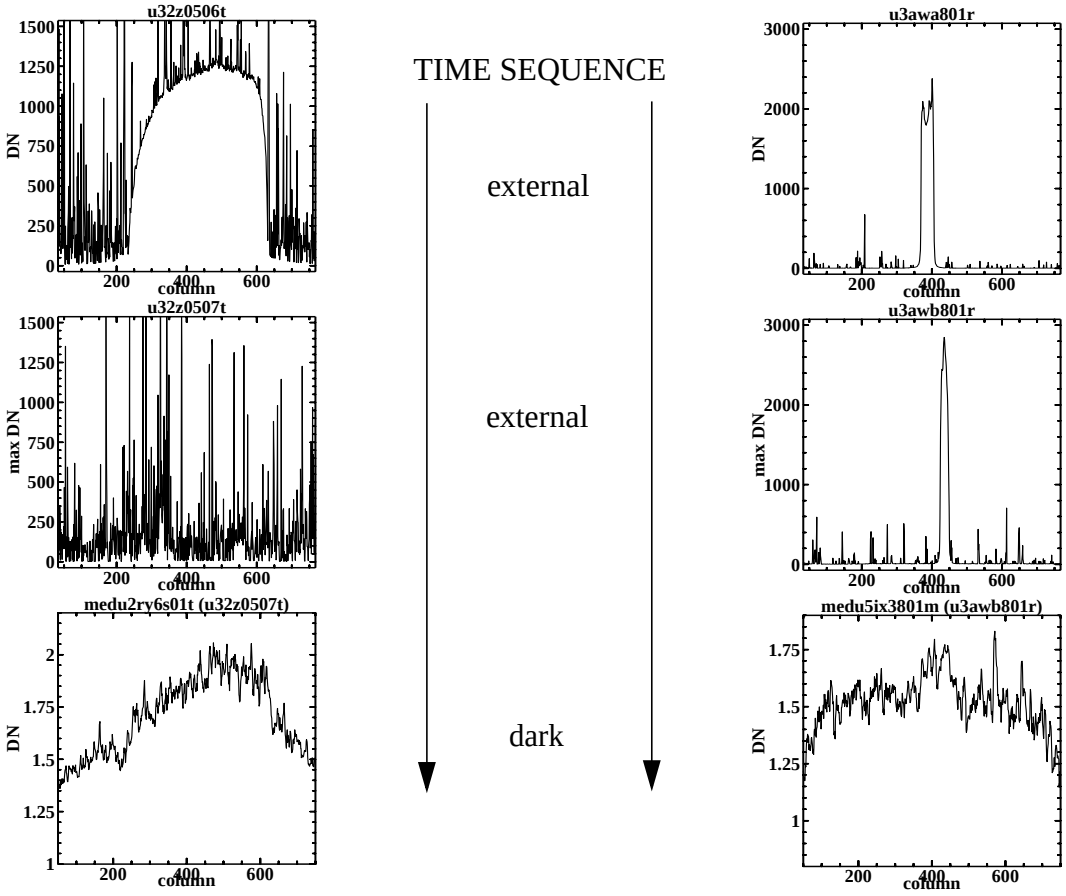

As in Biretta & Mutchler (1997), we analyze the relationship between maximum intensity and residual level data in natural log-natural log parameter space; the results are illustrated in Figure 3. The upper left panel presents all the good data (unshaded rows from Table 1); the other three panels present the good data in 2 year bins. The images with questionable residuals are included on the plot as small circles; these points were included in the fits but with very low weight. The residual level and the maximum target intensity level appear correlated; the formal fit to all the good, weighted data is

ln(residual) = -3.82 (+/-0.10) + 0.36(+/-0.01) * ln(Imax)

While the formal uncertainty is small, the large scatter in the data suggests the true uncertainty in the slope is 0.2 or 0.3. To determine whether the mix of long and short darks was contributing to the large scatter, we scaled the residuals in the short darks to those in the long darks by adding 0.6 (the natural log of the ratio of the exposure times) to the ln(residual) of each short dark, and recomputed the fit. However, the resulting slope and scatter in the data were not significantly different from the fit reported above.

Though sparse, the data does appear to follow the new fit in all time bins. It could be argued that the 1996/1997 data points appear to follow a steeper relationship than the points from other years, however, this could be just small number statistics. There does not appear to be any major evolution in the relationship over time, in marked contrast to other CTE components (Biretta et al., 2000). The CTE measured on cosmic rays, for example, undergoes a factor of ~4 increase between 1995 and 1999 (Riess et al., 1999).

The new fit is substantially shallower than the original 1.00*ln(Imax) (Biretta & Mutchler, 1997); this may be due to the use of median-filtered dark frames here and/or the larger number of images available now, together with the large scatter of individual points.

As an alternate technique, we also measured the residual and dark levels directly from the dark images, rather than from the median-filtered images. To circumvent the cosmic ray problem, we used the STSDAS testwfpc ‘gsky’ routine. The gsky computes the image mode as it does for the STSDAS WFPC2 ‘crrej’ task: it bins the pixel data, finds the most populated bin and fits a parabola to it and its two neighboring bins, thereby effectively clipping out most pixels affected by cosmic rays without changing the overall image levels as median filtering can. Here, the error bars represent ~0.05 DN errors in the residual and dark level measurements, which was the typical spread in gsky measurements taken around the chip (avoiding the droop area at the CCD edges). The results are presented in Figure 4, which shows the natural log of the residual measured via ‘gsky’ as a function of the natural log of Imax. The weighted formal fit to the data measured with ‘gsky’ is

ln(residual) = -7.84(+/-0.04) + 0.65(+/-0.01) * ln(Imax)

Figure 3: Correlation of residual in the dark with maximum intensity in the preceding external image; line is formal fit to weighted data. Upper left panel: all good data, along with the new best fit; data from 94-95, 96-97, and 98-99, are in lower left, upper right, and lower right panels, respectively. Images with very small residuals are included on the plot as small circles; these points were included in the fits but assigned very low weight.

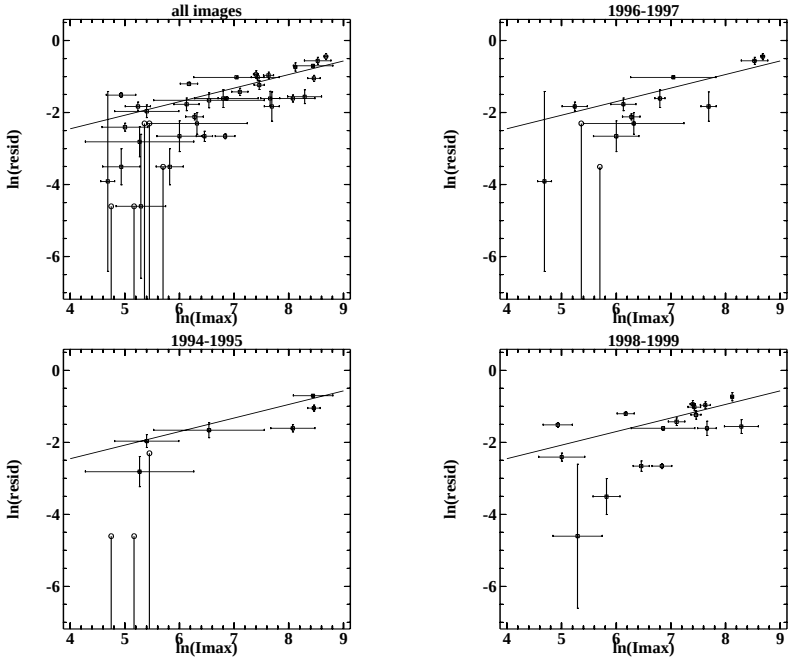

Figure 4: Correlation of residual in the dark, measured via STSDAS task gsky, with maximum intensity in the preceding external image; line is formal fit to weighted data.

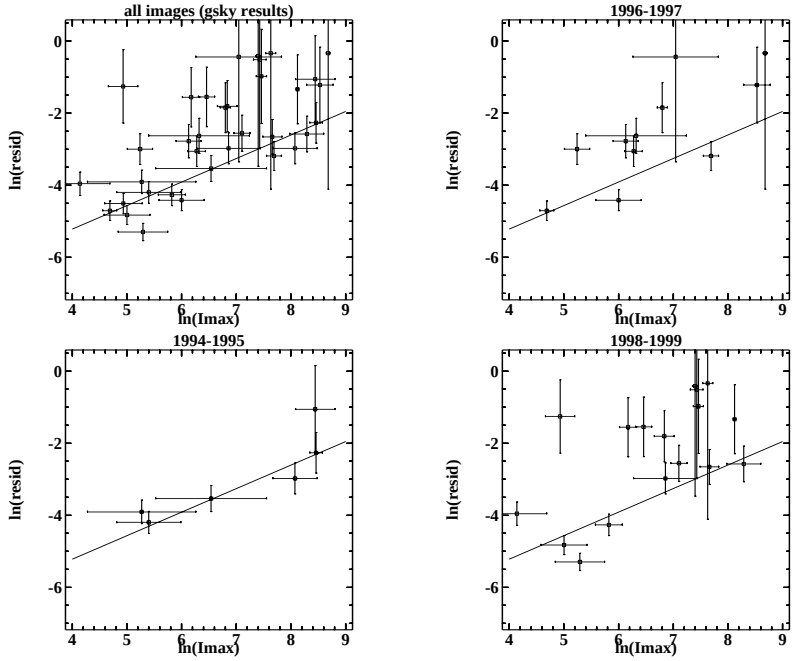

We also investigated the possibility that the charge trapping on these relatively long time scales (minutes) is due not to CTE but to residual bulk image (RBI). The RBI effect is thought to be caused by light redder than 6000 Å being trapped in the chip substrate (Thomsen, 1989). In this case, the trapped charge might appear as a function of wavelength, though the lumogen coating on the WFPC2 CCDs, which converts wavelengths shortward of 4800 Å to 5100-5800 Å, complicates the situation. Therefore, any RBI effect might only be apparent as an offset between residual image levels shortward and longward of 6000. Figure 5 presents the ln(residual), normalized to ln(Imax), as a function of wavelength; lines are unweighted medians of the data blueward and redward of 6000 Å. There appears to be a very slight effect but the averages are the same to within the errors (-0.30 +/-0.18 for blue vs. -0.39+/-0.28 for red); given the sparse data and large scatter, no firm conclusion can be reached.

Figure 5: Residual level in the dark as a function of wavelength.

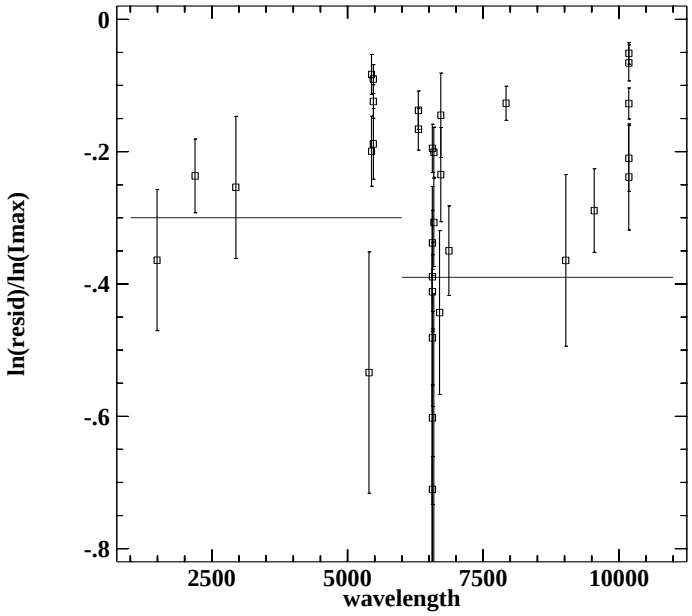

Conclusions

New data has been used to check the status of long time scale charge trapping in the WFPC2 CCDs via residual images in dark calibration frames. The additional data support the original conclusion that the trapped charge is correlated with the maximum intensity clocked through the pixel. Furthermore, the amount of trapped charge appears to have remained stable over the 6-year time span of the images. This is in contrast to the short time scale trapping where a large increase has been seen over the years (Whitmore & Heyer, 1997; Whitmore et al., 1999; Riess et al., 1999). No firm conclusion concerning the presence of a wavelength-dependent RBI component in the residuals can be drawn from this data. And finally, we note that there is evidence that the residuals can be relatively long-lived: there are some residuals clearly due to images taken more than 20 minutes before the dark.

References

Biretta, J., Baggett, S., and Riess, A., CTE Calibration Workshop, Jan 31-Feb 1,2000.

Biretta, J., and Mutchler, M., 1997, “Charge Trapping and CTE Residual Images in the WFPC2 CCDs,” ISR 97-05.

Biretta, J., Ritchie, C., and Rudloff, K., 1995, “A Field Guide to WFPC2 Image Anomalies,” ISR 95-06.

Holtzman, J., and the WFPC2 Team, 1995, PASP 107, 156.

Mutchler, M., O’Dea, C., and Biretta, J., 1998, “Analysis of the excess charge in WFPC2 overscans,” TIR 98-02.

Riess, A., Biretta, J., and Casertano, S., 1999, “Time Dependence of CTE from Cosmic Ray Trails,” ISR 99-40.

Thomsen, B., “Subtle Features in the Performance of P8603/S”, 1989, from CCDs in Astronomy, PASP Conference Series 8, edited by G. Jacoby.

Whitmore, B., and Heyer, I., 1997, “New Results on Charge Transfer Efficiency and Constraints on Flat-Field Accuracy,” ISR 97-08.

Whitmore, Bradley; Heyer, Inge; Casertano, Stefano, 1999, PASP 111, 1559.

Appendix A. Catalog of images and darks used in fits. Darks appear below their associated external images.

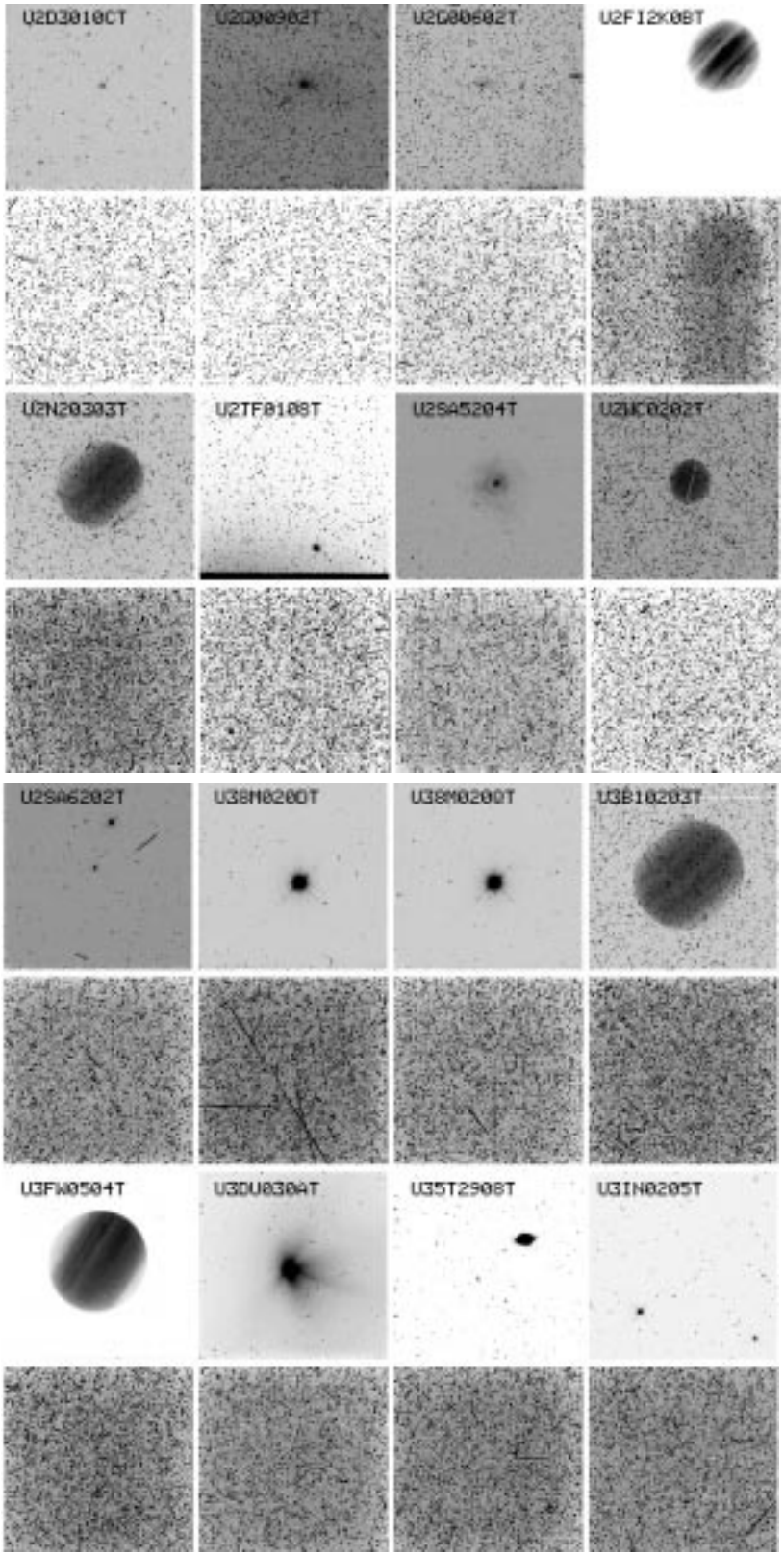

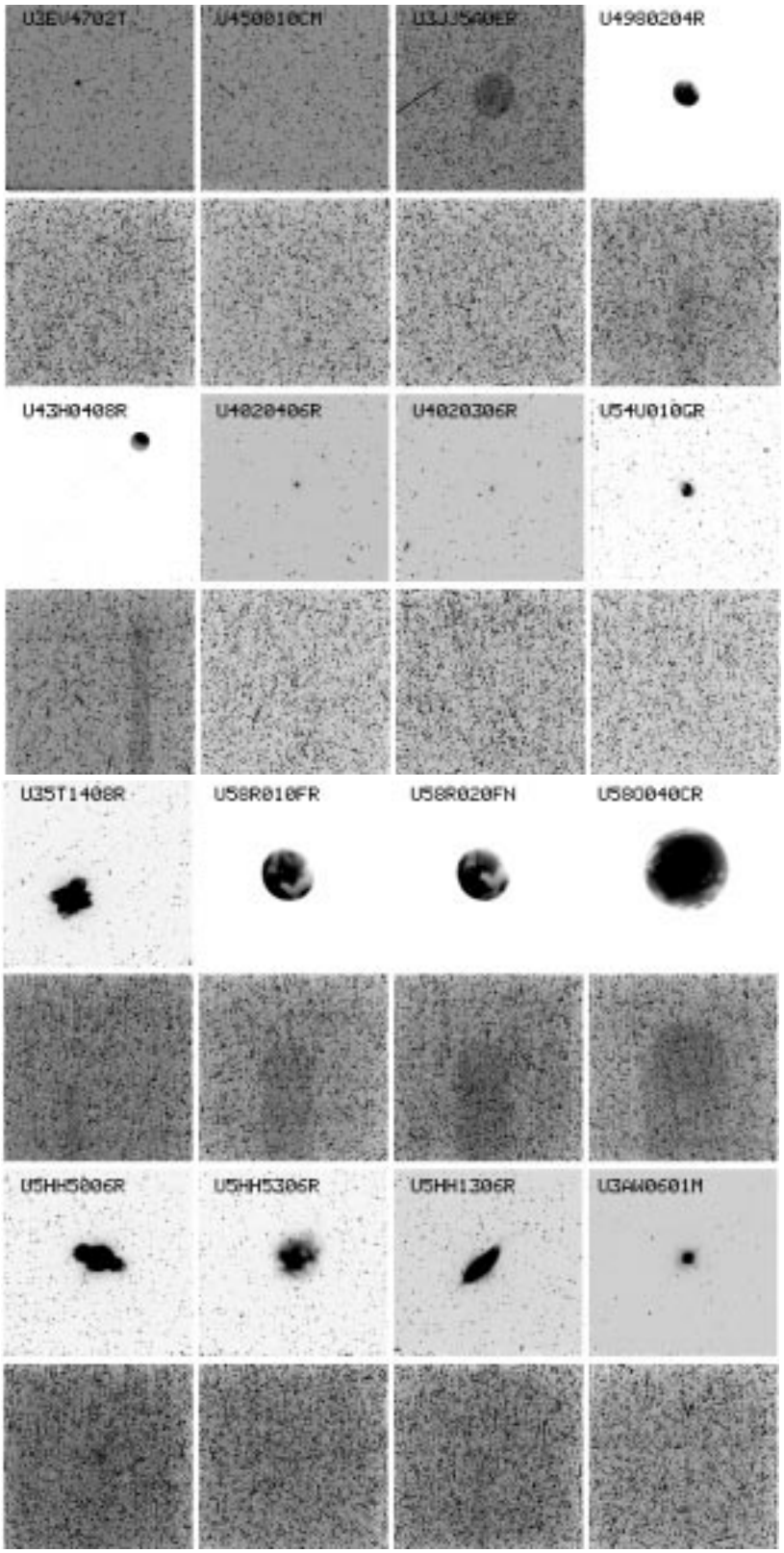
U3EV4702T
U450810CM
U3JJ540EP
U4980204R
U43H0408R
U4020406R
U4020306R
U54U010GR
U35T1408R
U58R010FR
U58R020FN
U580040CR
U5HH5006R
U5HH5306R
U5HH1306R
U3A40601M

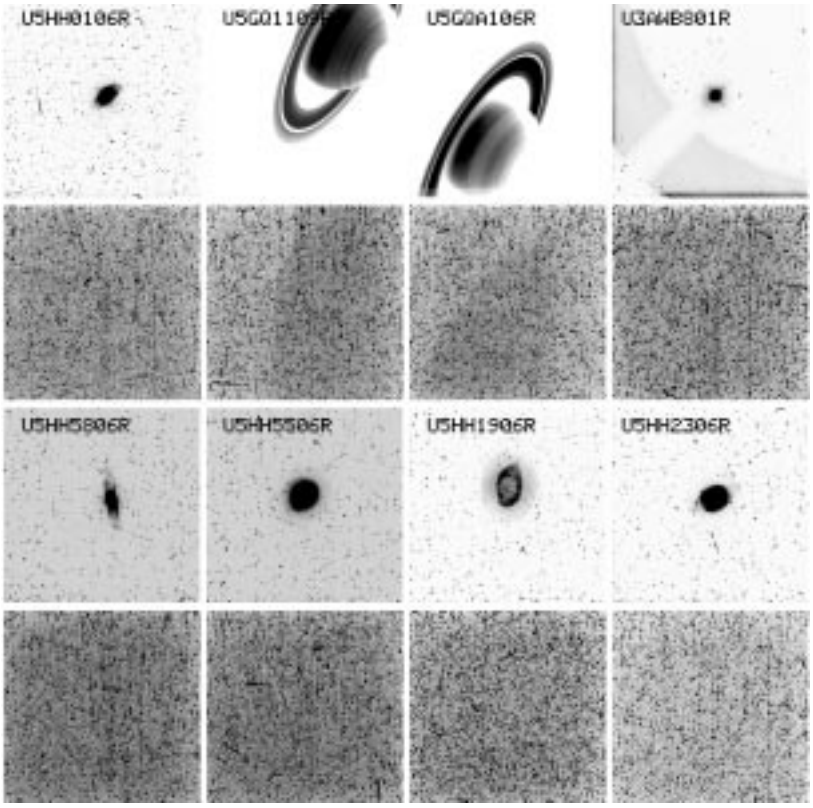
U5HH0106R
U5G0A106R
U3AWB801R
U5HH5806R
U5HH5506R
U5HH1906R
U5HH2306R

Appendix B. Plots of Imax from external images and average residuals from median-filtered darks. Each dark profile appears below the profile of the associated external image. When residual image features are difficult to identify, vertical bars mark column location of the external target on the dark profile (i.e., expected location of any residual feature).

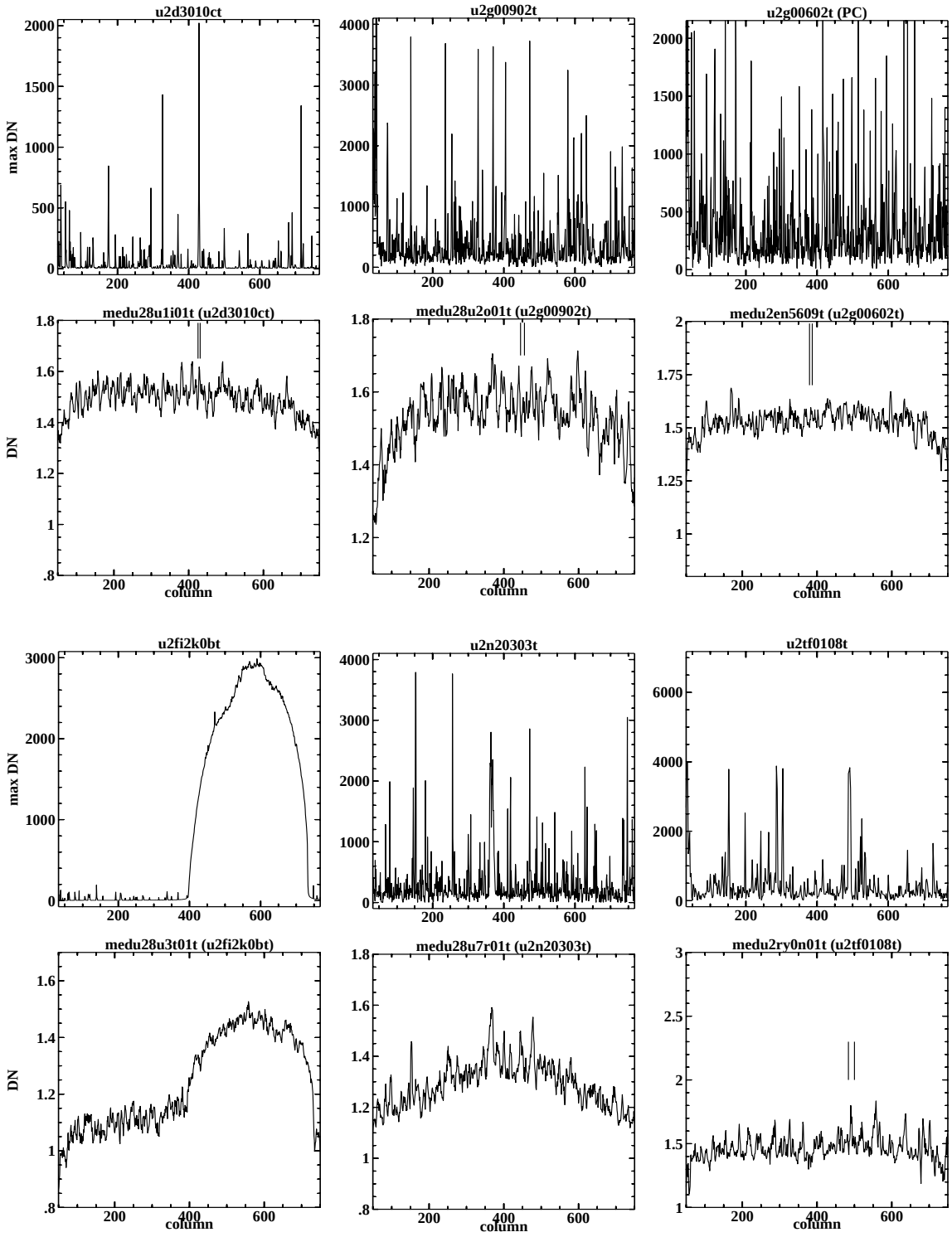

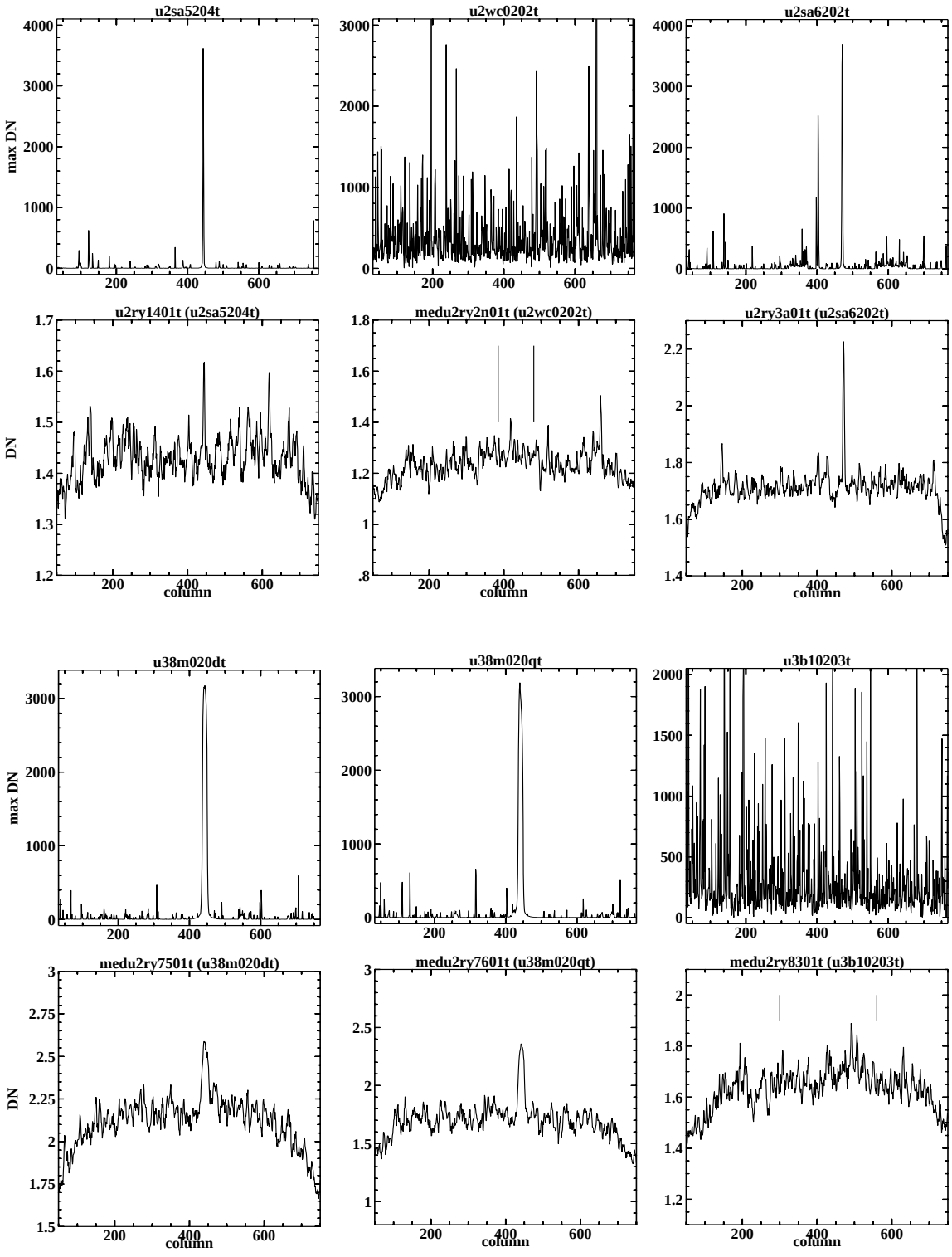
u2sa5204t
u2wc0202t
u2sa6202t
max DN
u2ry1401t (u2sa5204t)
medu2ry2n01t (u2wc0202t)
u2ry3a01t (u2sa6202t)
DN
column
u38m020dt
u38m020qt
u3b10203t
max DN
medu2ry7501t (u38m020dt)
medu2ry7601t (u38m020qt)
medu2ry8301t (u3b10203t)
DN
column

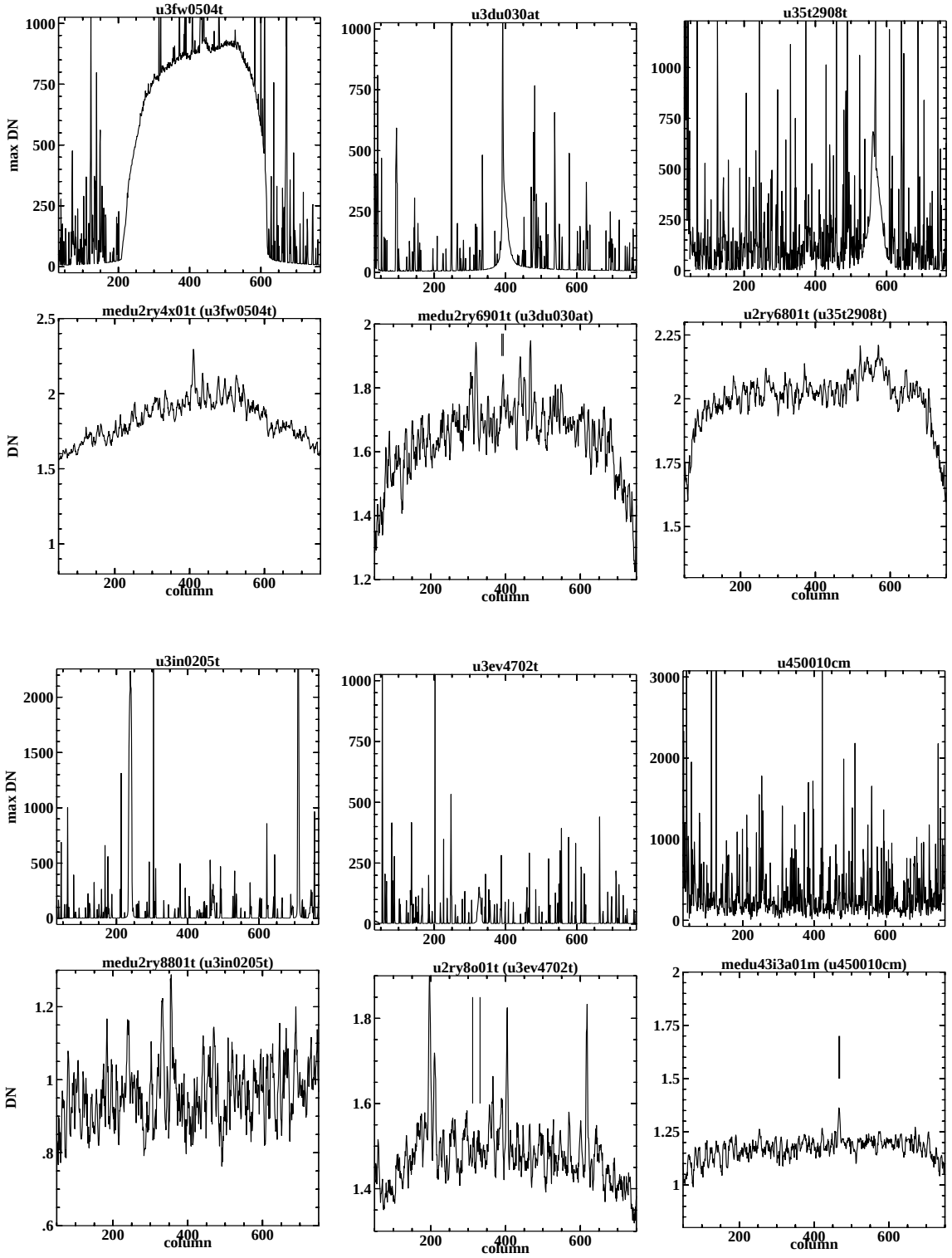
u3fw0504t
u3du030at
u35t2908t
max DN
medu2ry4x01t (u3fw0504t)
medu2ry6901t (u3du030at)
u2ry6801t (u35t2908t)
DN
column
u3in0205t
u3ev4702t
u450010cm
max DN
medu2ry8801t (u3in0205t)
u2ry8o01t (u3ev4702t)
medu43i3a01m (u450010cm)
DN
column

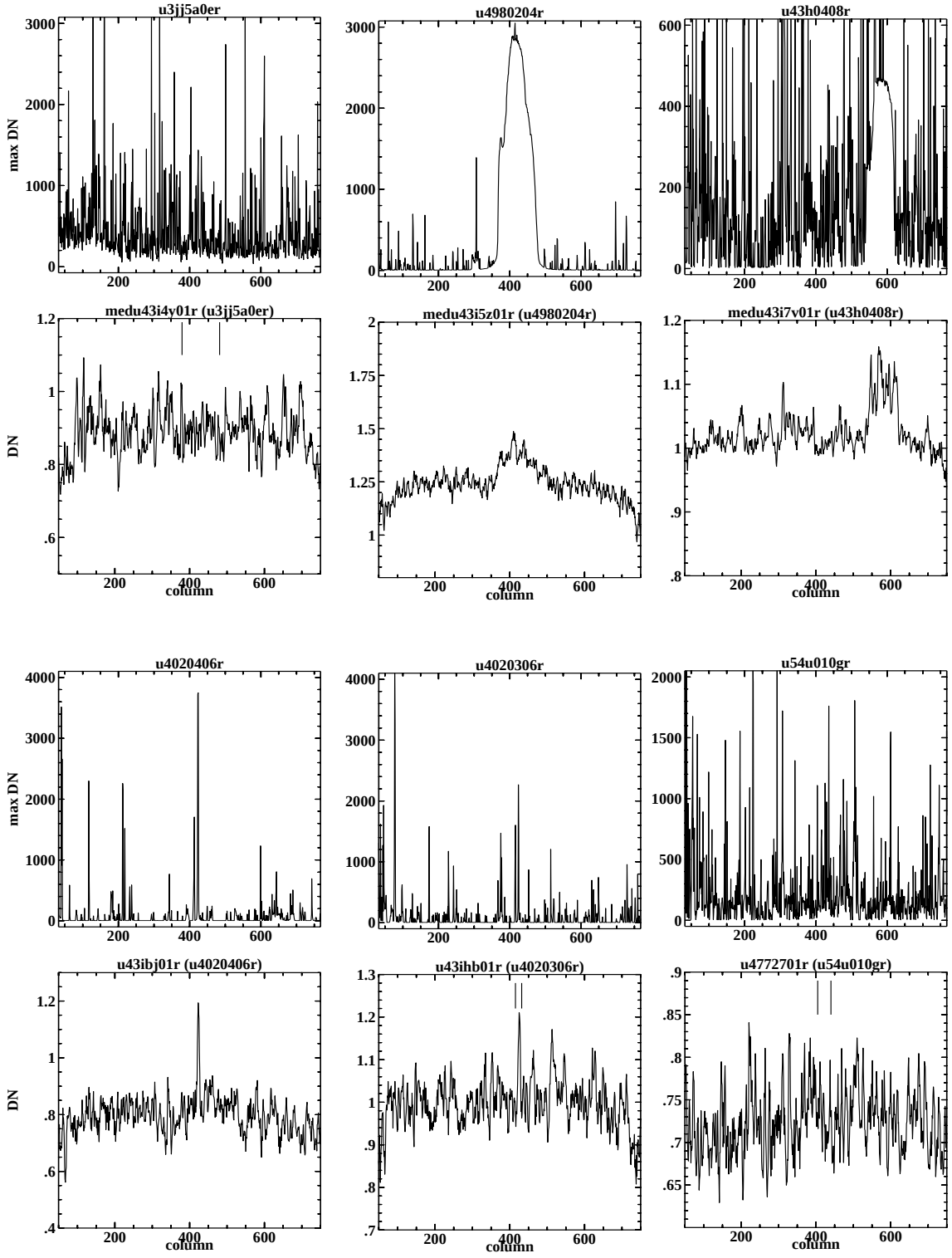
u3jj5a0er
u4980204r
u43h0408r
max DN
medu43i4y01r (u3jj5a0er)
medu43i5z01r (u4980204r)
medu43i7v01r (u43h0408r)
DN
column
u4020406r
u4020306r
u54u010gr
max DN
u43ibj01r (u4020406r)
u43ihb01r (u4020306r)
u4772701r (u54u010gr)
DN
column

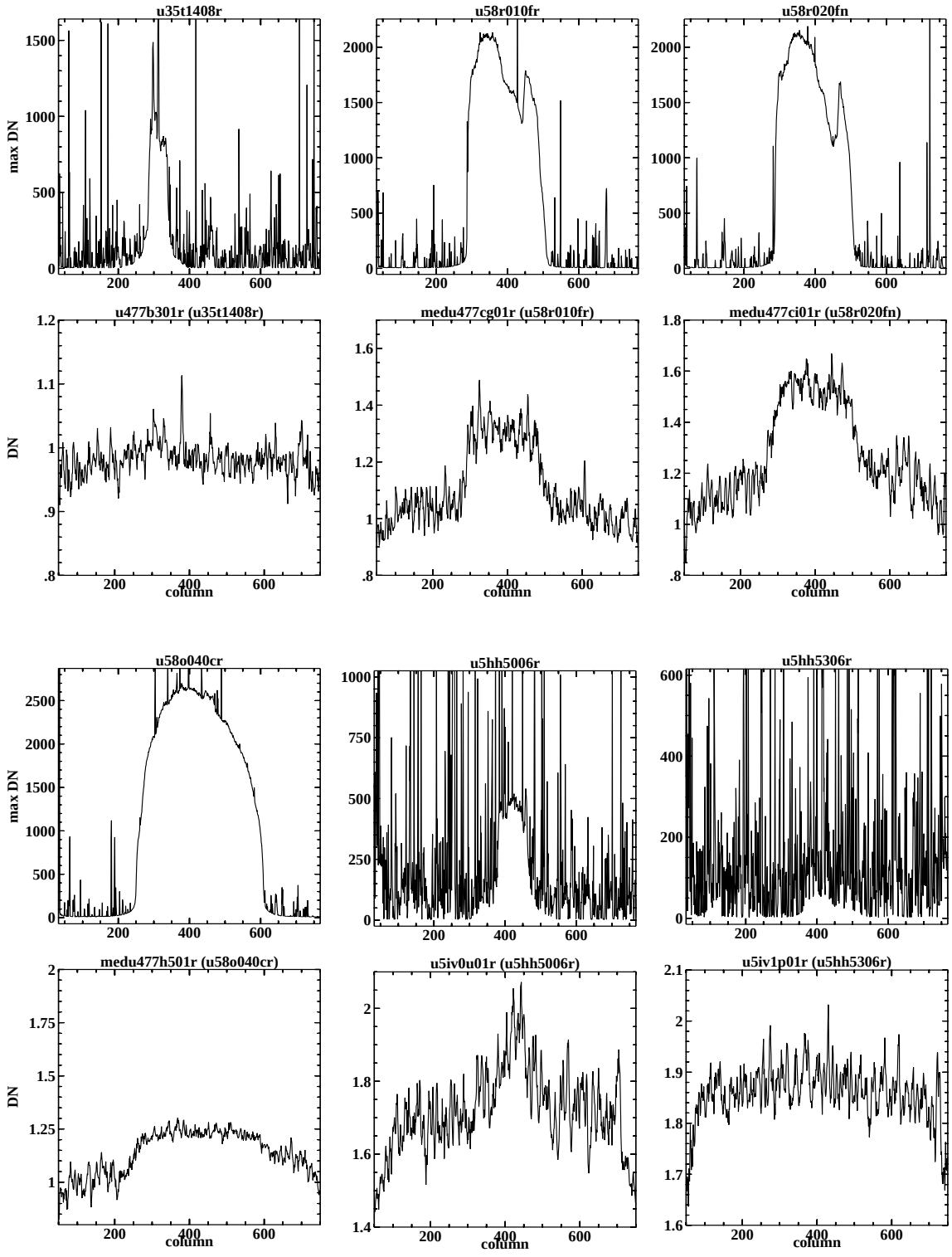
u35t1408r
u58r010fr
u58r020fn
max DN
u477b301r (u35t1408r)
medu477cg01r (u58r010fr)
medu477ci01r (u58r020fn)
DN
column
u58o040cr
u5hh5006r
u5hh5306r
max DN
medu477h501r (u58o040cr)
u5iv0u01r (u5hh5006r)
u5iv1p01r (u5hh5306r)
DN
column

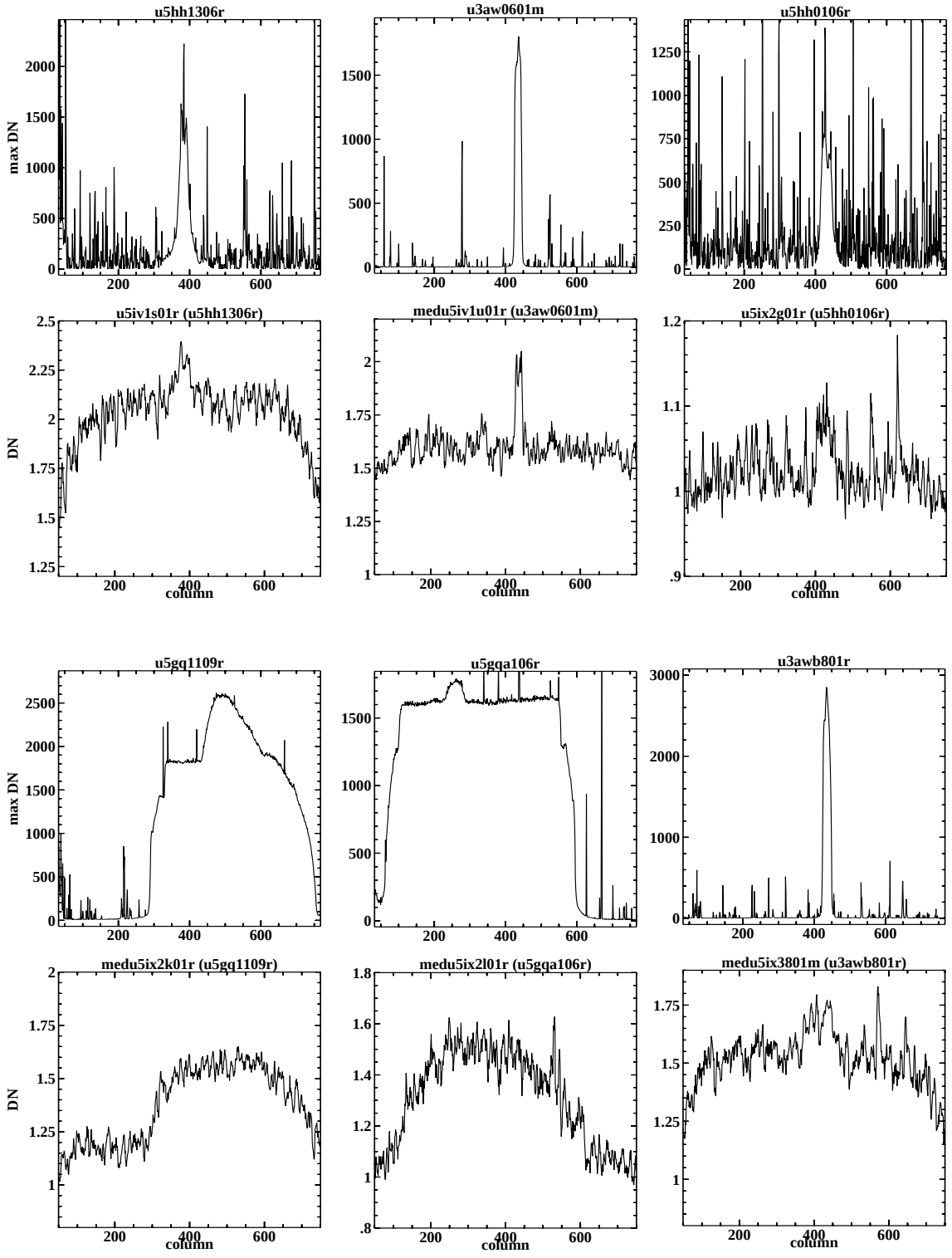
u5hh1306r
u3aw0601m
u5hh0106r
max DN
u5iv1s01r (u5hh1306r)
medu5iv1u01r (u3aw0601m)
u5ix2g01r (u5hh0106r)
DN
column
u5gq1109r
u5gqa106r
u3awb801r
max DN
medu5ix2k01r (u5gq1109r)
medu5ix2l01r (u5gqa106r)
medu5ix3801m (u3awb801r)
DN
column

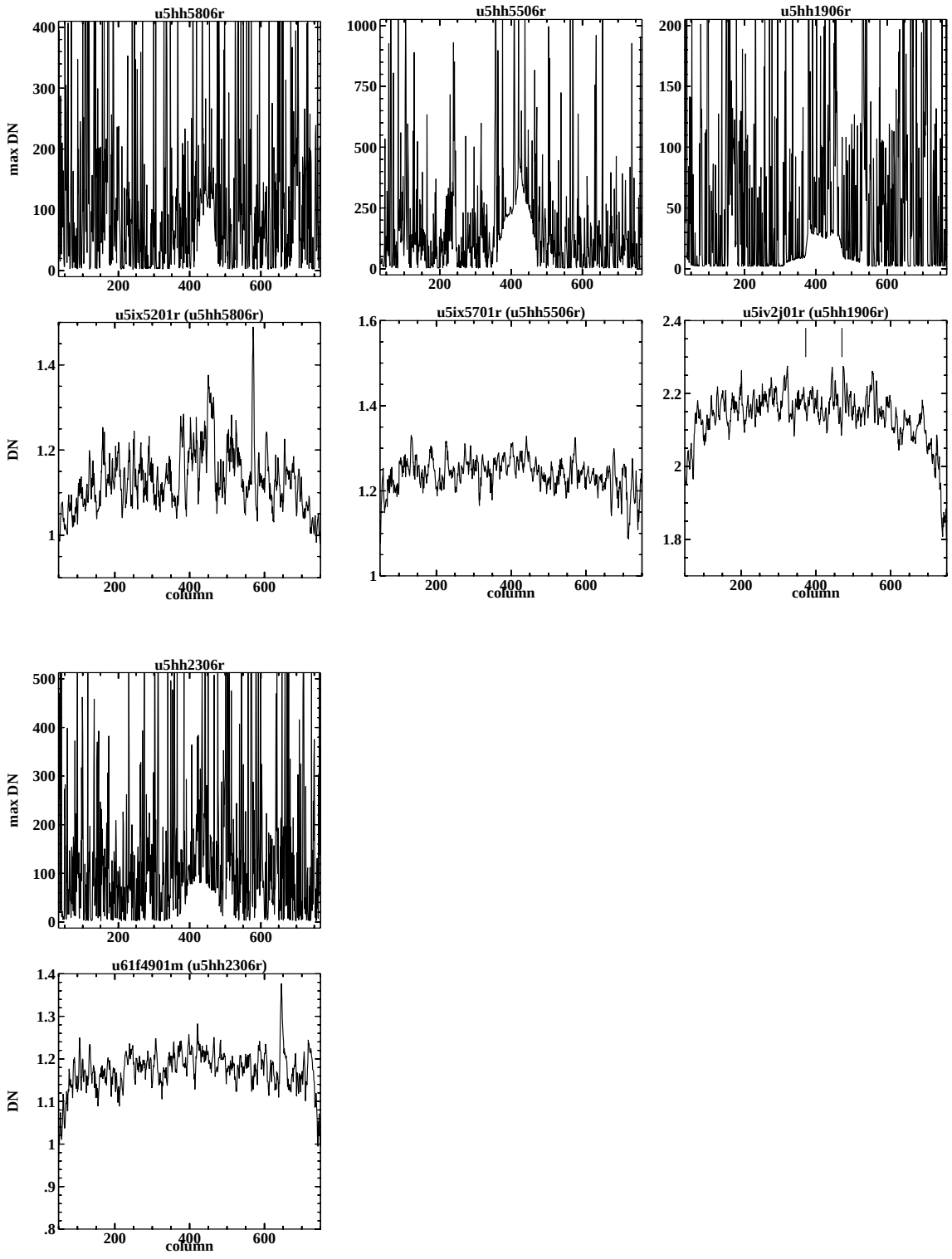
u5hh5806r
u5hh5506r
u5hh1906r
max DN
u5ix5201r (u5hh5806r)
u5ix5701r (u5hh5506r)
u5iv2j01r (u5hh1906r)
DN
column
u5hh2306r
max DN
u61f4901m (u5hh2306r)
DN
column